RSC Advances

ROYAL SOCIETY OF CHEMISTRY

www.rsc.org/advances

Designing binder-free, flexible electrodes for high-performance supercapacitor based on pristine carbon nano-onions and its composite with CuO nanoparticles

Debananda Mohapatra, Subramanya Badrayyana, Smrutiranjan Parida*

Department of Metallurgical Engineering and Materials Science, Indian Institute of Technology, Bombay, Mumbai – 400076, India

*Corresponding author

E-mail: paridasm@iitb.ac.in

Abstract

The increasing demand for energy has triggered tremendous research efforts for the development of light-weight and durable energy storage devices. This requires exploring simple, economical methods of preparation of the active materials and to design lightweight, flexible, free standing supercapacitor electrodes in an inexpensive binder-free process. Herein, we try to address both these critical issues using CNOs and it's composite with CuO as active materials. Active materials were supported on cotton wipes by a simple "sonication and drying" process to obtain light weight, flexible and free standing binder-free electrodes. In a symmetrical two electrode cell, pristine CNO electrode delivers a specific capacitance of 102.16 F/g (20 mV/s), energy density of 14.18 Wh/kg and power density of 2448 W/kg, which are the highest values reported so far for CNO based materials. CNO-CuO nanocomposites demonstrate very significant specific capacitance of 420 F/g (10 mV/s) with deliverable energy and power density at 58.33 Wh/kg and 4228 W/kg, respectively. Electrodes of both the active materials show excellent cyclic performance and stability, retaining upto 90-95% of initial capacitance after 5000 charge-

discharge cycles at a current density of 5 A/g. A simple cost estimation indicates that our device can deliver an energy density of 58.33 Wh/kg at an estimated cost of less than 1$.

1. Introduction

In recent years, there have been tremendous research efforts with the strong objective to increase the energy density, power density and cyclic performance of supercapacitors so that it can reach upto the level of batteries at lower fabrication cost. Supercapacitors also known as the ultracapacitors or electrochemical capacitors have been a potential attention from both industry and academia due to their superior rate capability, high power density, long cyclic performance, simple principle and low maintenance cost.[1] A fast growing market for portable electronic devices such as smartphones, notebooks, cameras, etc. are becoming more multifunctional requiring novel, lightweight, inexpensive, flexible and wearable electronic devices.[2,3]

It has been strongly recommended that it is critical to follow the best practices and methods to get reliable performance data using devices which mimics the real one. These include 1) measuring the performance with not too low scan rate or discharge current 2) using two-electrode practical testing cells instead of three-electrode measurements, which could overestimate the intrinsic result.[4,5] We want to emphasize that our performance data are based on the practical industry devices with electrode capacitance calculated using the recommended most reliable method rather than the three-electrode configuration. Voltage scan rates of at least 20 to 40 mV/s are needed to maintain discharge times on the order of a minute and adequately reflect a material's performance. Also, very low rates of discharge lead to large errors.

The materials used for the state-of-art supercapacitors include mainly three components, active material, conductive filler to enhance the overall conductivity and the binder material. It is noted

that conductive filler and binder takes about 10-20% of the total electrode weight, but hardly contributes to any capacitance performance. Hence, it's indispensable to design and develop a new, versatile and flexible binder-free electrodes for supercapacitor devices following the best practice methods to evaluate its performance.

As an important member of the fullerene family, CNOs, consisting of multiple concentric graphitic shells to form encapsulated structures, have been envisioned to be a promising supercapacitor electrode material with high power density due to nonporous outer shells that are easily accessible to electrolyte ions.[6] Despite their outstanding electrochemical properties, CNOs have not received adequate attention as an electrode material for supercapacitors because of the lack of convenient, cost-effective technique of preparation of CNOs in high yield. The methods developed so far to synthesize carbon onions suffer issues relating to purity, quantity, and quality. Ugarte showed that irradiating carbon soot with high-energy electron irradiation could result in carbon onions with closed caged cores that varied from a few layers to microns in size.[7] The drawback of the method included requirement of high energy input and it produced only minuscule amounts of CNOs. Thermal annealing of nanodiamond particles generated CNOs;[8] however, the need to use vacuum at high temperatures which required specialized equipment was the only drawback. Carbon arc plasma is another approach, in which one can fabricate gram amounts of onions; however, they are always contaminated by undesired byproducts, e.g. catalyst particles encapsulated in carbon cages.[9] Carbon arc discharges submerged in deionized water were also a step forward because the use of metallic catalysts was eliminated.[10,11] However, the products were a mixture of CNOs and nanotubes. Catalytic chemical vapor deposition route can be also a method for CNO production,[12] however the products are always contaminated by carbon encapsulates, similarly to carbon arcs. However, all these methods for

carbon nanostructure synthesis require high energy input and their yield of CNOs is low or species are obtained as a byproduct which cannot be separated easily from the product. Therefore, large-scale applications require a simple, continuous and energy-efficient method to synthesize nanostructures. A flame can naturally and easily produce an appropriate high-temperature environment with high radical concentrations required for the growth of CNOs. Therefore, flame synthesis shows a more promising potential for inexpensive and mass production of high-purity CNOs than other synthesis methods. Besides, the use of CNOs as a main electrode material for carbon supercapacitors shows rather moderate electrochemical performance (< 10 F g^{-1}).[13] Even activation and functionalization of CNOs failed to improve the performance of supercapacitor beyond 45 F g^{-1}.[6,14]

To address these issues, the focus is on designing and synthesizing composite electrode materials to exploit fully their advantages and overcome their individual disadvantages. Previous literature shows that high specific capacitance can be obtained if metal oxides are uniformly dispersed on carbon materials with high surface areas.[15-17] Combining carbon nanomaterials with metal oxides to prepare composites could enhance the specific surface areas, induce high porosity, facilitate electron and proton conduction, expand active sites, extend the potential window, protect active materials from mechanical degradation, improve cycling stability and improve the capacitive performance.[16,17] Among the transition metal oxides, CuO is noteworthy to explore as a promising supercapacitor material due to its low cost, abundant resources, non-toxicity, chemical stability, easy preparation and high theoretical capacitance (1800 F g^{-1}).[18,19] However, the poor electronic conductivity of CuO leads to the poor stability of repetitive cycling. By adding conductive carbon nanomaterials, the electronic conductivity of the CuO electrodes can be increased. Several journal publications on the fabrication of copper oxide composites with

various carbon allotropes for supercapacitor application are available in the literature.[20-22] The challenge, however, is to synthesize composites that are highly dispersible in polar solvents which can be easily loaded into the substrate. Also, highly dispersible composite nanoparticles improve the wettability of the electrodes. To address the aforementioned issues, we synthesized novel composite consisting of CNO and CuO nanoparticles. Combining CNO with copper oxide should lead to the manifestation of synergistic electrochemical properties from both of them. To the best of our knowledge, the synthesis of CNO-CuO nanocomposites and their electrochemical performance study has not been reported in the literature till date.

The other critical aspect in supercapacitor design is the way electrodes are prepared using particulate active materials. The pristine CNO powder is very difficult to handle, and the process of fabrication into an electrode is also tedious. Conductive agents (e.g. carbon black) and binders (e.g. poly (tetrafluoroethylene)) are always needed and have been used by many authors.[23-25] The use of binder masks the electrochemically active surface area and reduces the conductivity of the active material.[26] Recently, binder-free electrodes on conductive substrates for energy-storage have been explored.[27,28] But, complicated and costly synthesis processes have been used, which are not suitable for the large-scale production of supercapacitor devices. Therefore, it remains a great challenge to develop high-performance supercapacitor electrodes by a binder-free process that is facile, low-cost and scalable at room temperature.

In the present work, CNO and CNO-CuO nanocomposites were prepared by simple and economical methods. The composites were characterized by SEM, TEM, XRD, Raman and BET analysis. The supercapacitor performance of the flexible electrode materials was studied in a symmetrical two-electrode cell using aqueous electrolytes.

2. Experimental

2.1 Flame synthesis of CNOs

A simple flame synthesis method was implemented for the preparation of CNOs by using clarified butter (also known as *ghee* in Indian sub-continent region) as a precursor material.[29] In a typical experiment, a cotton wick, known as lamp wick, was soaked in clarified butter by placing it in a spirit lamp. The exposed end of the lamp wick was ignited in the ambient atmosphere. A clean, polished bronze plate was placed at the upper part of the flame to collect the soot. The soot from the flame deposited on the surface of the polished bronze plate. The yield depends on the duration of the collection (soot deposition on the collector) and the amount of precursor material (clarified butter). The method is capable of producing CNOs at the rate of grams of CNO per hour.

2.2 Preparation of CNO-CuO Composite

The CNO-CuO composite was prepared by a hydrothermal reaction. 50 mg of CNO powder was dispersed in 50 ml of DI water, 25 mg of copper acetate monohydrate was added to it and then the complete mixture was sonicated for 1 h. The obtained mixture was transferred to a Teflon-lined stainless steel autoclave and heated for six hours at 150 °C. After completion of the chemical reaction, the formed black suspension was washed and centrifuged several times. After washing, the precipitate was oven dried for 8 h at 70 ° C.

2.3 Fabrication of free-standing, flexible and binder-free electrodes

Free-standing, flexible and binder-free electrodes are prepared by a simple “sonication and drying” method using cotton wipes as support for active materials. 20 mg of CNO-CuO composite powder was dispersed in 10 ml of ethanol to maintain a concentration of 2 mg/mL.

The dispersion was sonicated for 30 minutes in a bath sonicator to form a binder-free CNO-CuO ink. A cotton wipe of 2 x 2 cm dimension was dipped into the binder-free CNO-CuO ink and soaked for a few minutes. The ink with the wipe was then sonicated for a fixed time. During the process, the active materials uniformly and conformally coat the fabrics of the wipe. The mass loading of CNO-CuO composite on the wipe depends on the time of sonication, which was optimized to obtain the required mass loading. After the loading process, the electrode was completely dried at 70 °C in a hot air oven. The mass of the loaded CNO-CuO was obtained by taking the difference of weight before and after loading. A similar procedure was followed to prepare CNO electrodes.

The active material loaded on the cotton wipe electrodes showed excellent mechanical properties, which can be folded and stretched without the detachment of the CNO or the composite particles from the electrode (Fig. S1).

2.4 Materials Characterizations

The microscopic morphology of pristine CNOs and composite electrodes were characterized using a Hitachi Model S-3400N field-emission gun scanning electron microscope (FEG-SEM) and a JEOL TEM-2100 high-resolution transmission electron microscope (HR-TEM) with 0.19 nm point resolution. Raman spectra were collected from 100-4000 cm^{-1} in Horiba HR8000 spectrometer equipped with argon laser of wavelength 514.4 nm. Nitrogen adsorption and desorption experiments were carried out at 77 K on ASAP 2020 V3.05 H volumetric adsorption analyzer. Before the collection of the isotherm the sample is degassed at 300 °C for 20 h under vacuum. The specific surface area (SSA) is calculated by multipoint Brunauer Emmett Teller (BET) method. The pore-size distribution is obtained from the adsorption data by using the Barret-Joyner-Halenda (BJH) method.

2.5 Electrochemical Measurements

All the electrochemical measurements were performed in a two electrode symmetric cell configuration assembled into a Swagelok cell. Two active electrodes were separated by a tea bag cloth soaked in 1 M Na_2SO_4, which acts as a separator. Electrochemical performances of the device were studied by cyclic voltammetry (CV) and galvanostatic charge−discharge (GCD) measurements using Biologic Potentiostat SP-300. All the CV tests were done between –1 and +1 V at different scan rates of 10-200 mV/s. Galvanostatic charge/discharge curves were measured in the potential range –1 to +1 V at different current densities of 2-15 A/g. The cyclic stability of supercapacitor was tested at a constant applied current density of 5 A/g in the voltage range −1 to +1 V for 5000 cycles.

3. Results and discussions

3.1 Morphological and Structural Characterization

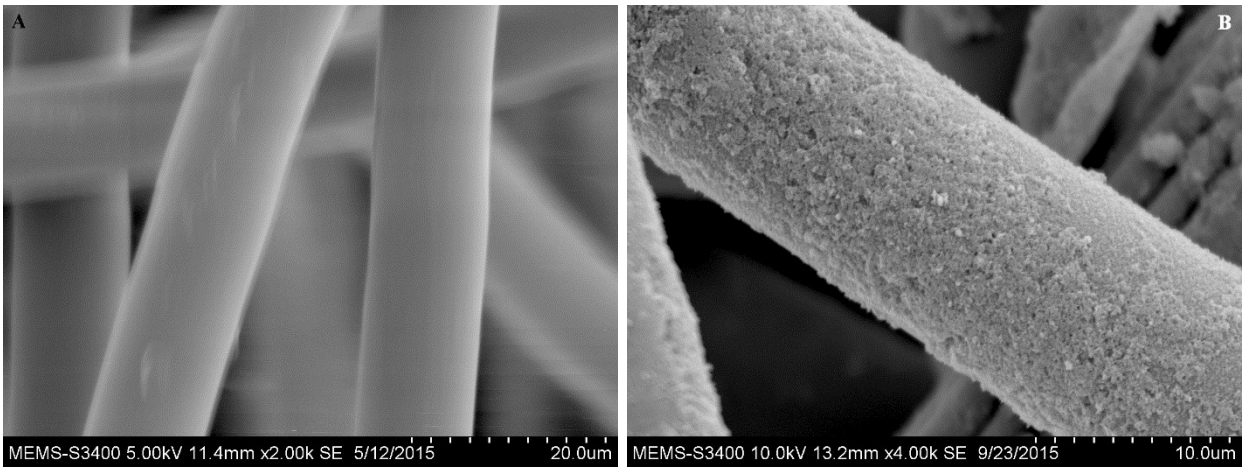

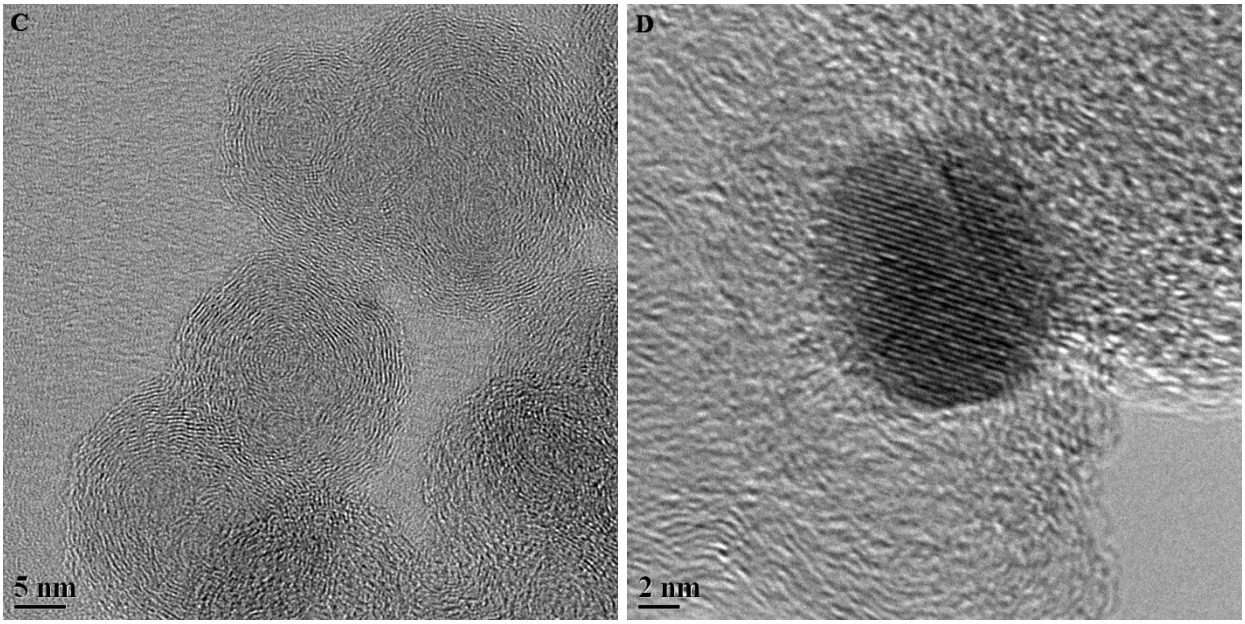

Fig. 1 SEM images showing the cotton wipe **(A)** without active material coating and **(B)** with conformal CNO-CuO coating. HRTEM micrographs of as-prepared **(C)** CNOs and **(D)** CNO-CuO composite.

The SEM micrograph of cotton wipe before and after composite coating are presented in Fig. 1A and 1B. The wipe textile consists of numerous interwoven cellulose fibers, forming a hierarchical structure with complicated surface morphology resulting in pores of various length scales. The hierarchical porous structure of the wipe allows high mass loading of the active material. The SEM image reveals the uniform conformal coating of pristine CNO (Fig. S2) and CNO-CuO composite particles (Fig. 1B) on the fibers of the cotton wipe. The cotton fibers in the wipe are primarily made of cellulose and contain hydroxy functional groups.[28] The CNO particles used in this study are also funtionalized with oxygen containing functional groups, which form hydrogen bonding with the –OH group of the fiber. Besides, there is Van-der-Waals interactions between the active materials and the fiber.[28] Because of these two types of

interactions CNO and CNO-CuO nanoparticles are conformally coated on the fibers of the cotton wipe.

The microstructural features of the as-prepared CNOs and CuO-CNO composite have been investigated by HR-TEM analysis and are presented in Fig. 1C and 1D, respectively. From Fig. 1C, the concentric shells of graphitic layers are visible with an interlayer spacing of 0.334-0.353 nm, which is a characteristic feature of CNOs. The average size of the CNO nanoparticles vary between 35-40 nm. On examining the composite (Fig. 1D), presence of different phases (i.e. CNO and CuO) is evident which is an indication of the composite formation. The lattice spacing was measured to be 0.228 nm corresponding to the (111) planes of monoclinic CuO.[30] The intershell spacing between the concentric graphitic layers in the composite was same as that of pure CNO.

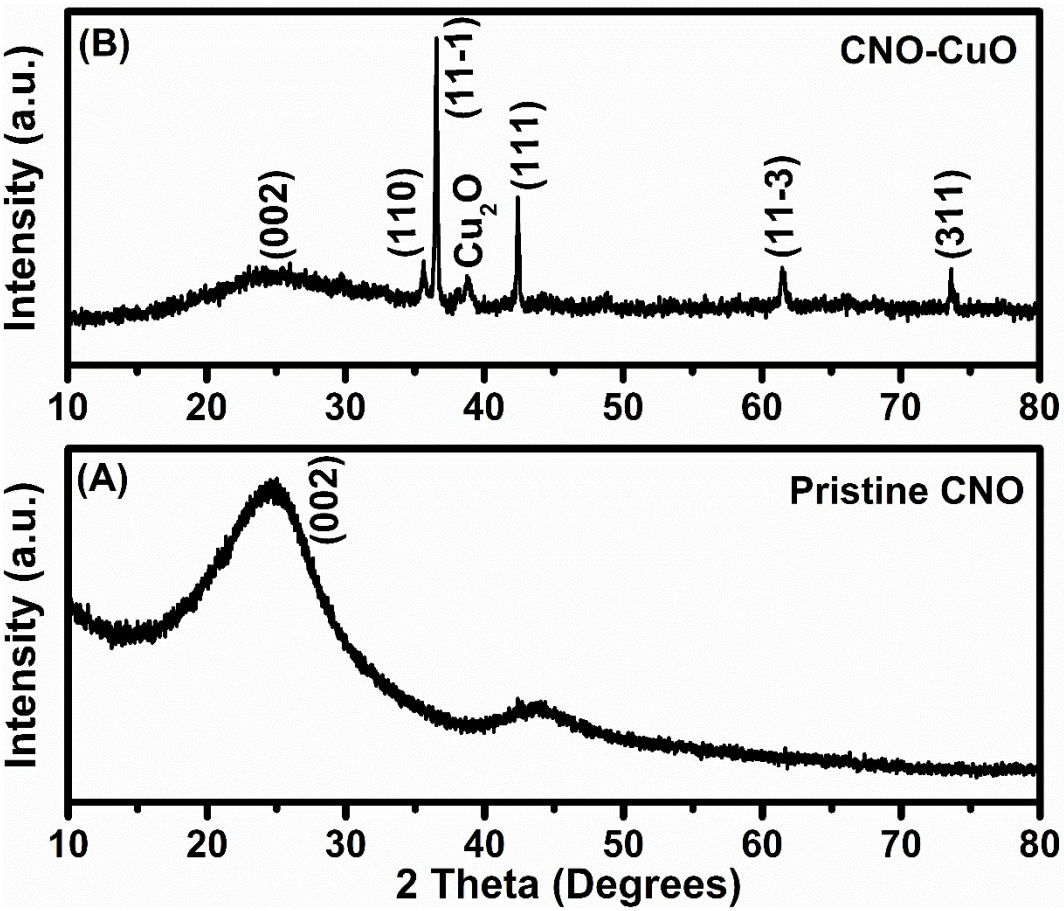

Fig. 2 XRD spectra of as prepared CNOs and CNO-CuO composite.

Crystal structure and phase purity of active materials were investigated by XRD. The XRD of as-prepared composite material and pristine CNO (Fig. 2) shows a prominent graphitic peak at 2θ = 25.5° corresponding to the (002) reflection of the graphitic plane. The broadness of the (002) peak in CNO can be attributed to the small size of the CNOs and a relatively short domain order of the stacked graphitic layers.[31] The low intense peak between 2θ = 40° and 50° in the XRD of CNO corresponds to either (100) or (101) reflection. In the composite, observed peaks can be indexed to the monoclinic phase of CuO (JCPDS card no. 05-661).[20] The existence of traces of Cu_2O phase in the XRD pattern of the composite are detected, which may have formed due to the low reaction temperature (150 °C) used in our experiment.

The formation mechanism of CuO can be explained on the basis of different growing rates of various crystal facets. The coordination number of Cu^{2+} is generally six in a hydrolysis reaction. Each Cu^{2+} ion is surrounded by six water molecules when copper salt is dissolved in water, in which four water molecules surround Cu^{2+} to form a planar square structure, and other two water molecules are located at its axis leading to octahedral $Cu(OH)_6^{4-}$ growth units. The binding energies of two OH^- located at axis is lower than those of OH^- located at plane.[32] So the two OH^- located at axis are easily replaced and dehydrated to form CuO crystallites i.e., the growth rates of CuO crystal in axis are higher than those of plane. Therefore, the difference in growth rates of various directions is emerged and leads to the formation of anisotropic CuO nanocrystals. Furthermore, in the process of crystals growth, the Gibbs free energies of crystallites surfaces are usually very high, and the crystallites have the tendency to aggregate together to decrease the Gibbs free energies of the surfaces.[33] Consequently, the secondary aggregation of small CuO crystallites leads to the formation of aggregating spherical structure. The as-prepared CNO by flame synthesis of clarified butter is highly dispersible in water i.e., hydrophilic and hence it doesn't precipitate in the hydrothermal process. Hence the doping efficiency can be controlled and quantified easily.

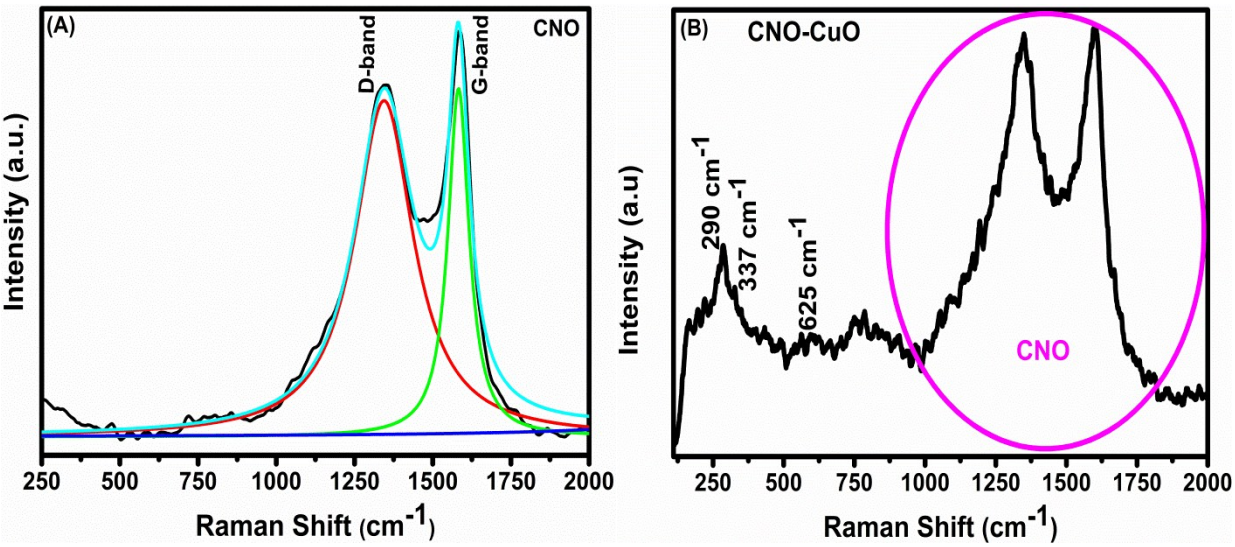

Fig. 3 Raman spectra of as prepared **(A)** CNOs and **(B)** CNO-CuO composite.

Raman analysis of CNOs and CNO-CuO composite are presented in Fig. 3A and 3B, respectively. Raman analysis allows identification of various forms of carbon as well as fingerprints for single layers, bilayers and few layers reflecting changes in the electron bands of graphitic carbon.[34] The peak positioned at 1344 cm^{-1} designated as D-band, which from various defects present in the CNOs lattice. The peak positioned at 1582 cm^{-1} originates from the ordered sp^2 hybridized carbon. The narrowness of the G-band in CNO points to the high degree of perfection of the graphitic network in the concentric shells. The broad nature of D and G-band in CNO-CuO composite indicates the presence of smaller graphitic fragments, which is in agreement with XRD results. The degree of disorderness in spherical graphitic nanostructures can also be estimated by the intensity ratio of D and G-bands (I_D/I_G). I_D/I_G for CNOs is 0.94 indicating surface defects due to various oxygen-containing functional groups.[35] For the composite, this ratio decreases to 0.92 indicating a decrease in the surface defects due to the reaction of the oxygen-containing functional groups with copper acetate for the formation of CuO nanoparticles. This suggests the composite materials have fewer defects, indicating better

electrical conductivity than the prisine CNOs. The composite formation is confirmed by appearance of bands at 290, 337 and 625 cm^{-1} (Fig. 3B) which are due to vibrations in the CuO lattice.[22] With reference to the vibration spectrum of single CuO crystal, the peak at 290 cm^{-1} can be assigned to the A_g mode, whereas peaks positioned at 337 and 625 cm^{-1} can be assigned to the B_g modes.[30]

N_2 adsorption/desorption isotherms obtained at −196 °C was employed to estimate the SSA and pore size distribution of CNO and CNO-CuO composite. From the multipoint BET measurements, the SSA of the as-prepared CNOs was found to be 144.26 m^2/g. It is seen that the as-prepared CNOs exhibits type–IV isotherm with a hysteresis at higher relative pressure, indicating the presence of mesopores (Fig. S4A).[25] The pristine CNOs exhibit a bimodal pore size distribution i.e., they contain mesopores and macropores ranging from (2–100 nm), with the majority of pores having a diameter around 2-10 nm and 30-100 nm (Fig. S4B). The presence of macropores in the sample can be due to the existence of inter-cluster and intra-cluster pores in the CNO nanoparticles. After composite formation with CuO, the corresponding BET surface area slightly decreases to 60.7 m^2/g (Fig. S4C). But the pore-size distribution (Fig. S4D) indicates majority of micropores (from 0.6 to 1 nm) which is an added advantage as it will enhance the capacitance.[36]

3.2 Electrochemical Characterization

Fig. 4 shows the cyclic voltammograms of as-obtained flexible CNO electrodes as well as CNO-CuO composite in 1 M Na_2SO_4 at different sweep rates within the potential range of −1 to +1 V in a two electrode symmetrical cell configuration (Fig. 4A and 4C).

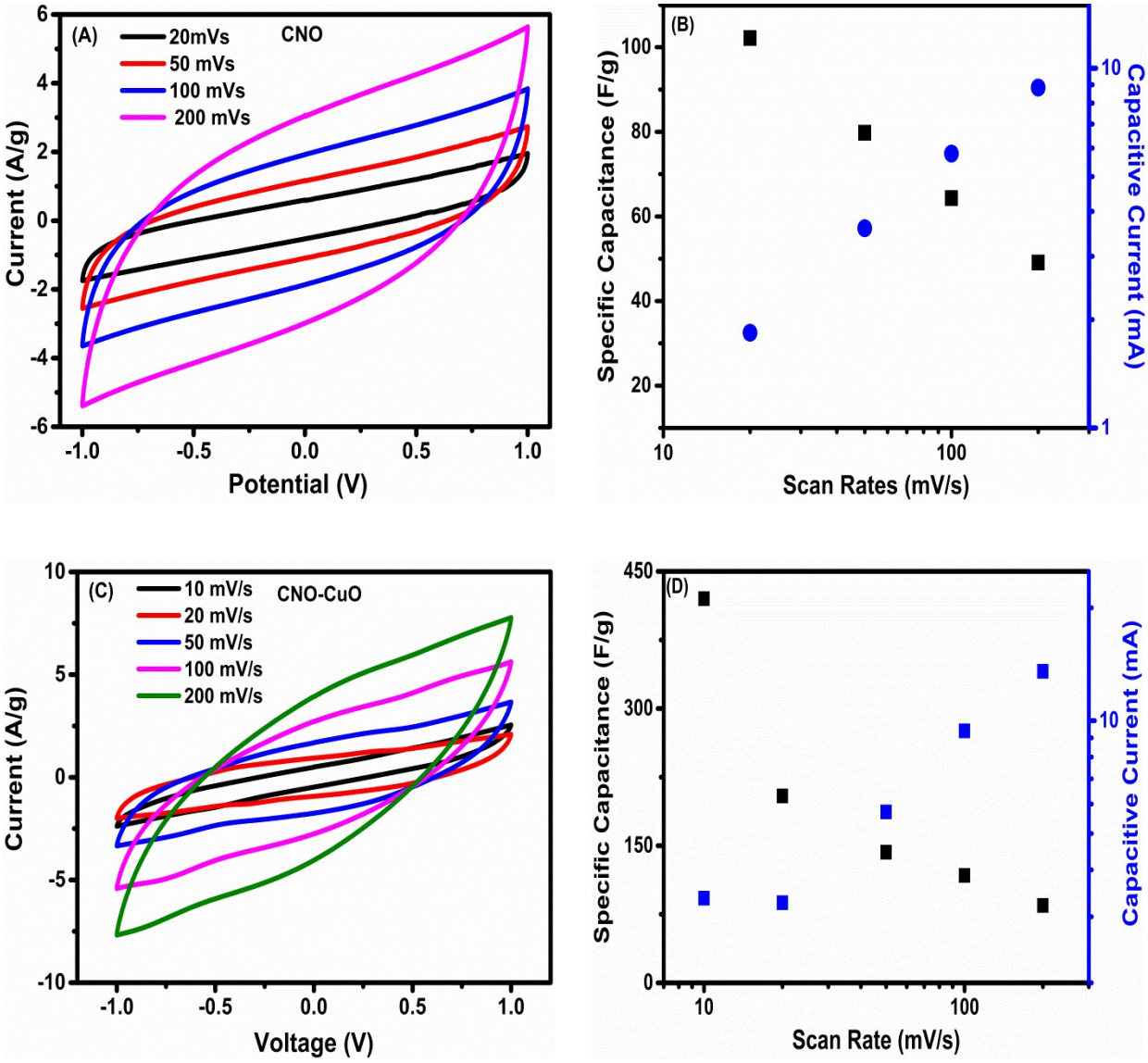

Fig. 4 (A) Cyclic voltammograms of pristine CNOs at the scan rates of 20-200 mV/s in 1 M Na_2SO_4 electrolyte **(B)** The relationship between specific capacities, scan rates and capacitive currents for pristine CNO electrodes **(C)** Cyclic voltammograms of CNO-CuO composite at the scan rates of 10-200 mV/s in 1 M Na_2SO_4 electrolyte **(D)** The relationship between specific capacities, scan rates and capacitive currents for CNO-CuO

It is observed that the voltammograms of pristine CNOs from a scan rate of 20 mV/s to 200 mV/s in Fig. 4A do not show any redox peaks, which evidently establish that the supercapacitive

behavior is free from any faradaic reactions. The quasi-rectangular shapes of the CV curves are an indication of ideal electrical double layer capacitive behavior with excellent electrochemical stability under given conditions. The symmetry and shape of the curve remain unaffected even at a high scan rate of 200 mV/s (Fig. 4B), indicating the excellent rate capability. The symmetric rectangular nature of the CV curves indicates compatibility of electrolyte ion size/pore size.[13]

The specific capacitance has been calculated by equation (1);

$$Cs = 2 * \left(\frac{I}{Scan\ Rate\ \left(\frac{dv}{dt}\right) * V * M} \right) \quad \ldots\ldots\ldots\ldots\ldots\ldots\ldots\ldots\ldots\ldots\ldots\ldots\ldots\ldots \text{(1)}$$

where,

I = Average current during the anodic and cathodic sweep.

V = Potential window

M = Weight of the active electrode material coated on one of the electrodes (g)

In symmetrical 2-electrode cell configuration, flexible and binder free CNO electrodes demonstrated a specific capacitance of 102.16 F/g. This is the highest value reported for pristine CNOs in a two-electrode cell configuration. Important to note that these reported capacitance values are at 20 mV/s, which is considerably higher than the reported scan rates in the literature.[15,37] As reported by Stoller and Ruoff, for any practical application a higher capacitance at higher scan rate is desired.[4] For non-functionalized, non-activated pristine CNOs, our result is highly competitive and higher by several factors of magnitude than that reported in the literature.[6,15,24,38-42] The as-synthesized CNO is highly hydrophilic and hence can be easily dispersed in water to form an ink which can be conformally coated onto the cotton fabric by a simple “sonication and drying” process. The wipe textile consists of numerous interwoven

cellulose fibers, forming a hierarchical structure with complicated surface morphology resulting in pores of various length scales. The hierarchical porous structure of the wipe allows higher mass loading of CNO per square centimetre. Both these factors contribute for the higher capacitance of CNO than other reported literature. It is important to note that most of the specific capacitance values reported in the literature are measured in three electrode configuration, which overestimates the capacitance value by a factor of two.[4]

From Fig. 4A and 4B, when scan rate increases, the capacitive current increases causing a slight asymmetry of the CV curve. The asymmetry in CV curves at higher scan rate may be due to the saturation of ions inside the pores of CNO electrode, which increases the internal resistance of the electrode restricting faster ion diffusion. On the other hand, at low scan rates, the charge accumulation process is slow, due to which electrolyte can access most of the surface area of the electrode. This increase in the electro-active surface area results in high specific capacitance.

Fig. 4C depicts the CV profile of CNO-CuO composite at different scan rates from 10 to 200 mV/s. As we observe from the obtained CV curves, there is a pseudocapacitive contribution from CuO along with the double layer contribution from CNO in the composite electrode. Specific capacitance as high as 420 F/g was obtained for the CNO-CuO, which is by far the highest value reported till date for any composite based on CuO and carbon nanomaterials following the best practice methods of evaluation. The remarkable enhancement in the specific capacitance of the composite material can be attributed to the synergistic effect of both components i.e., the high electrical conductivity of CNO and the pseudocapacitance of CuO. The intact assembly between the CNO and the CuO nanoparticles after composite formation, results in an intimate interaction of both components, enhancing charge transfer between the two components by introducing new paths for electron transfer and leading to rapid redox reactions of the CuO nanoparticles. The

effective charge transfer in the electrode played an important role in enhancing the specific capacitance and rate capability. Further, the microporous nature (pore size < 1 nm) of the composite material also contributes for enhanced capacitance.[36]

In all measurements, there is a common trend of decreasing C_s values with an increasing scan rates (Fig. 4B and 4D). It is a well-known trend that for very low scan rates, the C_s values are higher because the ions have a much longer time to penetrate and populate in all the available electrode surface and form electric double layers, which are needed to generate higher capacitance.[43]

There is a linear dependence of capacitive current with sweep rate in case of CNO (Fig. 4B). In other words, the votammetric currents are almost directly proportional to the sweep rates, which is an indication of pure double layer capacitive behavior. Whereas for CNO-CuO composite the capacitive current does not change linearly with scan rate (Fig. 4D) indicating Faradaic contribution to the capacitive behavior.

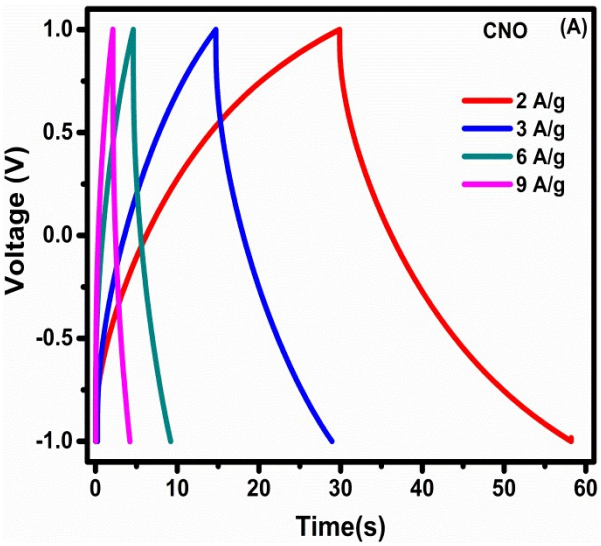

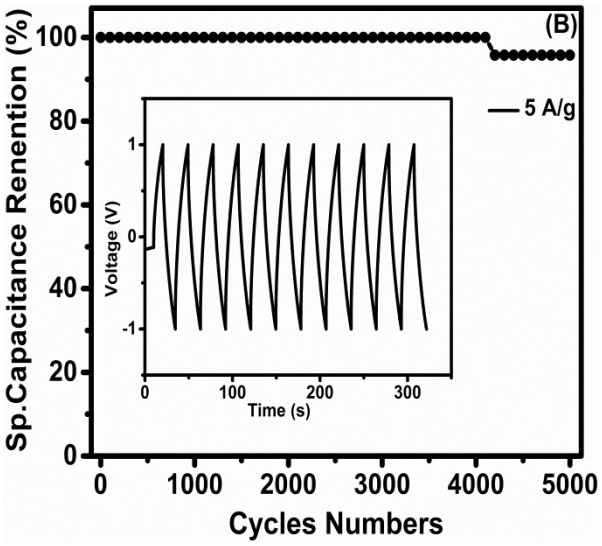

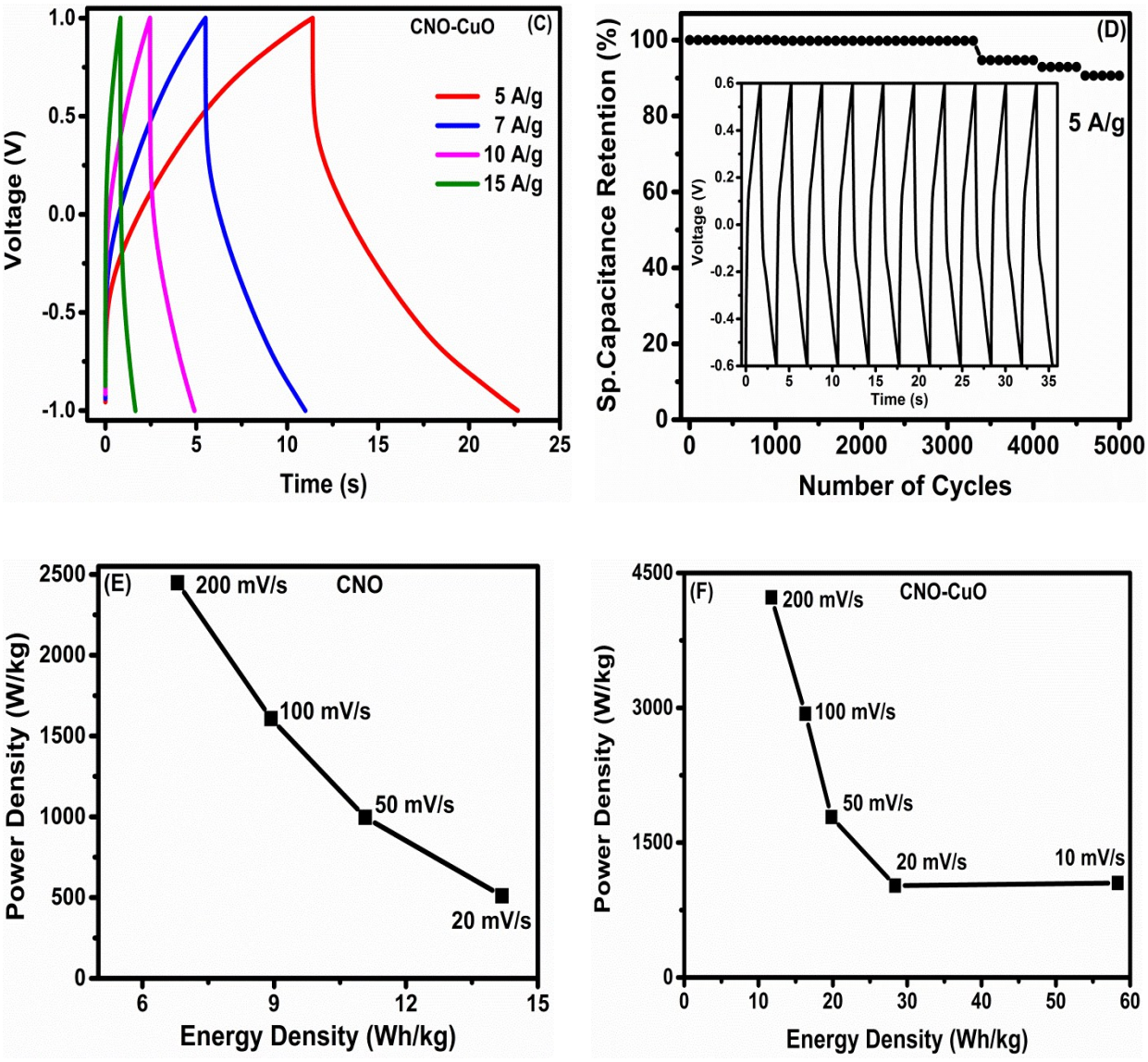

Fig. 5 (A) Galvanostatic charge-discharge (GCD) curves at different current densities of pristine CNOs **(B)** Cyclic stability of pristine CNOs **(C)** GCD curves at different current densities for CNO-CuO **(D)** Cyclic stability of CNO-CuO composite and Ragone plots of flexible **(E)** CNO based supercapacitor **(F)** CNO-CuO based supercapacitor.

Galvanostatic charging/discharging were carried out within the potential range of −1 to +1 V with varying current densities between 2−15 A/g and the measured results are shown in Fig. 5. The symmetrical and near linear slope was observed in the case of CNO at all current densities

indicating pure double layer formation (Fig. 5A). The electrodes show a coulombic efficiency greater than 90% demonstrating excellent electrochemical reversibility throughout the entire charge-discharge process. The GCD curves of CNO-CuO composite electrode (Fig. 5C) shows that the discharge curves are slightly distorted and slightly unsymmetric to their corresponding charging counterparts, indicating pseudocapacitive contribution.

The electrochemical stability of CNO and CNO-CuO composite electrodes were evaluated by performing charge-discharge experiments for 5000 cycles at a current density of 5 A/g, as shown in Fig. 5B and 5D, respectively. After 5000 cycles, the specific capacitance retention of the CNO and CNO-CuO composite electrodes are 95% and 90%, respectively, demonstrating excellent cyclic stability with a high degree of reversibility in repetitive charge/discharge process. The marginal capacitance loss may be due to the charge transfer limiting process that increases the internal resistance and eventually decreases the initial capacitance over repetitive cycling. In other words, there may be the blockage of electroactive sites due to electrolyte flooding or mass transport issues.[13]

The energy density and power density are very significant parameters for any energy storage device. Ragone plots are used to illustrate the energy density of a supercapacitor as a function of power density. The energy density and power density of pristine CNOs and CNO-CuO composite electrodes are calculated as per equations (2) and (3), respectively.

$$\textbf{Energy density } E_d \ (Wh\ \mathrm{kg}^{-1}) = \frac{1}{8} * Cs * V^2 \quad \text{..... (2)}$$

$$\textbf{Power density } P_d \ (W\ \mathrm{kg}^{-1}) = \left(\frac{Ed}{V}\right) * \left(\frac{dv}{dt}\right) \quad \text{..... (3)}$$

where,

C_s = Specific capacitance calculated from CV curves

V= Voltage window

$\left(\frac{dv}{dt}\right)$ = scan rate (V/s)

CNO electrodes show maximum performance with a highest energy density of 14.18 Wh/kg at a power density of 510.66 W/kg at 20 mV/s which gradually reduces to 6.8 Wh/kg at 2448 W/kg at a current density of 200 mV/s as depicted in the Ragone plot (Fig. 5E). However, the CNO-CuO composites show enhanced deliverable energy density up to 58.33 Wh/kg at a scan rate of 10 mV/s and power density of 4228 W/kg at a scan rate of 200 mV/s (Fig. 5F). The obtained values for composite are higher than either CNO or CuO values reported till date.[6,14,19,20]

To further investigate the redox behavior of the composite electrode we measured the electrochemical response in 1 M NaOH electrolyte (Fig. 6). Starting from scan rate of 5 mV/s to 200 mV/s, we observe a symmetric pair of both anodic and cathodic peaks over the entire scan range (Fig. 6A). This result indicates that there is a reversible Faradaic reaction of CuO during charging and discharging process. The main pseudocapacitive behavior of the composite sample can be attributed to the reversible redox transition of Cu^{2+} to Cu^{+} and vice versa.[37] Further, there is an almost linear dependence of capacitive current with scan rate (Fig. 6B).

The CNO-CuO composite showed a maximum specific capacitance of 638.09 F/g with a deliverable energy density of 31.9 Wh/kg and a maximum power density of 2360.7 W/kg in symmetrical 2-electrode cell configuration (Fig. 6C). This can be attributed to the homogeneous distribution of CuO nanoparticles over the CNO network, which introduces new paths for the electron transport and hence improve the conductivity and the capacitive behavior of the electrode.

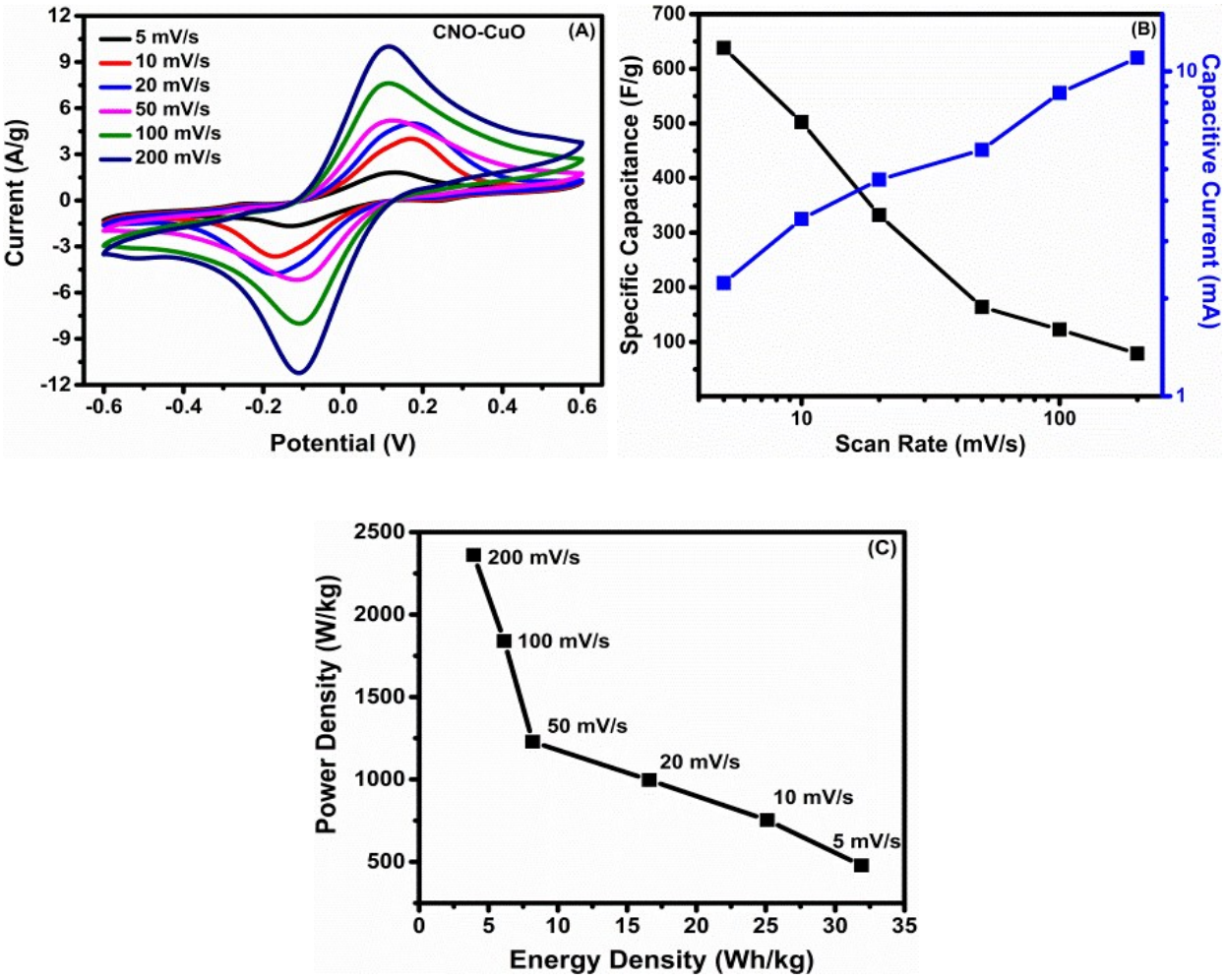

Fig. 6 (A) CV curves of CNO-CuO at scan rates of 20, 50, 100 and 200 mV/s in 1 M NaOH electrolyte **(B)** Variation of specific capacitance and capacitive current as a function of scan rate and **(C)** Ragone plot of flexible CNO-CuO based supercapacitor in 1 M NaOH

We have successfully demonstrated for the first time that free standing, flexible and binder-free CNO-based supercapacitors electrodes can be prepared by simple cost-effective fabrication method. To the best of our knowledge, there is no such reported device that uses simple and easily available materials like cotton wipes as substrate and tea bag as a separator, which shows high-performance characteristics. Based on the cost analysis (Table 1), we can claim that our device can deliver an energy density of 58.33 Wh/kg at an estimated cost of less than 1 $.

Table 1: Cost analysis for the supercapacitor device

Material	**Cost (INR)**
Cotton Wipe (Substrate)	01
Tea Bag (Separator)	01
Active Material (CNO-CuO Composite)	50
Electrolyte	05
Total	**57 (< 1$)**

4. Conclusions

Employing simple active material preparation technique and novel electrode fabrication method we have successfully enhanced the capacitance of the pristine CNO and CNO-CuO composite, following the best practice methods of evaluation. We have demonstrated for the first time a facile and scalable flame synthesis method to prepare highly dispersible and functionalized CNO nanoparticles. An extremely simple "sonication and drying" technique was used to develop binder free flexible electrodes using cotton wipes. A high specific capacitance of 102.16 F/g and a deliverable energy density of 14.18 Wh/kg and power density of 2448 W/kg was achieved for pristine CNO. The addition of redox surface functionality (CuO) led to a composite with more conductive networks, which exhibits higher capacitance (420 F/g), energy density (58.33 Wh/kg), power density (4228 W/kg) and cyclic stability (5000 cycles with more than 90% capacitance retention at 5 A/g) in 1 M Na_2SO_4 electrolyte. By changing the electrolyte to 1 M NaOH, the CNO-CuO composite showed a maximum specific capacitance of 638.09 F/g with a deliverable energy density of 31.9 Wh/kg and a maximum power density of 2360.7 W/kg in

symmetrical 2-electrode cell configuration. The novelty of this work is that our device can deliver an energy density of 58.33 Wh/kg at an estimated cost of less than one dollar.

Acknowledgements

This work was supported by financial assistance from the Industrial Research and Consultancy Center (IRCC), IIT-Bombay and DST (SERC). The authors acknowledge the access to experimental facilities at Centre for Research in Nanotechnology and Science (CRNTS) and Metallurgical Engineering and Materials Science (MEMS) Dept., IIT Bombay. We express our gratitude to Mrs.Aaradhana Pant for HRTEM imaging at CRNTS.

Notes and references

Electronic Supplementary Information (ESI) available: Fabrication of free-standing, flexible and binder-free electrodes, Morphology of CNO, Mechanical conditions of the electrodes after charge-discharge process, N_2 adsorption/desorption isotherms and pore size distribution of CNO and CNO-CuO composite, Synthesis and morphology of CuO nanoparticle. See DOI: 10.1039/x0xx00000x

1 J. Yan, Q. Wang, T. Wei and Z. Fan, *Adv. Energy Mater.*, 2014, **4**,1300816 .

2 Y. Liang, Z. Wang, J. Huang, H. Cheng, F. Zhao, Y. Hu, L. Jiang and L. Qu, *J. Mater. Chem A*, 2015, **3**, 2547-2551.

3 S. E. Moosavifard, M. F. El-Kady, M. S. Rahmanifar, R. B. Kaner, M. F. Mousavi, X. Tian, M. Shi, X. Xu, M. Yan, L. Xu, A. Minhas-Khan, C. Han, L. He and L. Mai, *Adv. Mater.*, 2015, **7**, 7476-7482.

4 M. D. Stoller and R. S. Ruoff, *Energy Environ. Sci.*, 2010, **3**, 1294–1301

5 Y. Gogotsi and P. Simon, *Science*, 2011, **334**, 917–8.

6 Y. Gao, Y. S. Zhou, M. Qian, X. N. He, J. Redepenning, P. Goodman, H. M. Li, L. Jiang and Y. F. Lu, *Carbon*, 2013, **51**, 52–58.

7 D. Ugarte, *Nature*, 1992, **359**, 707–709.

8 V. L. Kuznetsov, A. L. Chuvilin, Y. V. Butenko, I. Y. Mal'kov and V. M. Titov, *Chem. Phys. Lett.*, 1994, **222**, 343–348.

9 R. Selvan, R. Unnikrishnan, S. Ganapathy and T. Pradeep, *Chem. Phys. Lett.*, 2000, **316**, 205–210.

10 Sano N, Wang H, Chowalla M, et al, *Nature*, 2001, **414**, 506.

11 H. Lange, M. Sioda, A. Huczko, Y. Q. Zhu, H. W. Kroto and D. R. M. Walton, *Carbon N. Y.*, 2003, **41**, 1617–1623.

12 C. He, N. Zhao, C. Shi, X. Du, J. Li, L. Cui and F. He, *Scr. Mater.*, 2006, **54**, 1739–1743.

13 M. E. Plonska-Brzezinska and L. Echegoyen, *J. Mater. Chem. A*, 2013, **1**, 13703.

14 R. Borgohain, J. Li, J. P. Selegue and Y.-T. Cheng, *J. Phys. Chem. C*, 2012, **116**, 15068–15075.

15 M. E. Plonska-Brzezinska, D. M. Brus, A. Molina-Ontoria and L. Echegoyen, *RSC Advances*, 2013, **3**, 25891-25901.

16 X. Zhang, W. Shi, J. Zhu, D. J. Kharistal, W. Zhao, B. S. Lalia, H. H. Hng and Q. Yan, *ACS Nano*, 2011, **5**, 2013–2019.

17 A. Allagui, T. Salameh and H. Alawadhi, *J. Electroanal. Chem.*, 2015, **750**, 107–113.

18 B. Vidyadharan, I. I. Misnon, J. Ismail, M. M. Yusoff and R. Jose, *J. Alloys Compd.*, 2015, **633**, 22–30.

19 S. E. Moosavifard, M. F. El-Kady, M. S. Rahmanifar, R. B. Kaner and M. F. Mousavi, *ACS Appl. Mater. Interfaces*, 2015, **7**, 4851–4860.

20 V. Senthilkumar, Y. S. Kim, S. Chandrasekaran, B. Rajagopalan, E. J. Kim and J. S. Chung, *RSC Advances*, 2015, **5**, 20545–20553.

21 D. P. Dubal, D. S. Dhawale, R. R. Salunkhe, V. S. Jamdade and C. D. Lokhande, *J. Alloys Compd.*, 2010, **492**, 26–30.

22 A. Pendashteh, M. F. Mousavi and M. S. Rahmanifar, *Electrochim. Acta*, 2013, **88**, 347–357.

23 F. Béguin, K. Szostak, G. Lota and E. Frackowiak, *Adv. Mater.*, 2005, **17**, 2380–2384.

24 M. E. Plonska-Brzezinska, M. Lewandowski, M. Błaszyk, A. Molina-Ontoria, T. Luciński and L. Echegoyen, *ChemPhysChem*, 2012, **13**, 4134–4141.

25 B. Zhang, D. Wang, B. Yu, F. Zhou and W. Liu, *RSC Advances*, 2014, **4**, 2586.

26 C. Yuan, J. Li, L. Hou, X. Zhang, L. Shen and X. W. Lou, *Adv. Funct. Mater.*, 2012, **22**, 4592-4597.

27 G. Q. Zhang, H. Bin Wu, H. E. Hoster, M. B. Chan-Park and X. W. Lou, *Energy Environ. Sci.*, 2012, **5**, 9453.

28 L. Hu, M. Pasta, F. La Mantia, L. Cui, S. Jeong, H. D. Deshazer, J. W. Choi, S. M. Han and Y. Cui, *Nano Lett.*, 2010, **10**, 708–714.

29 N. C. Ganguli and M. K. Jain, *J. Dairy Sci.*, 1973, **56**, 19–25.

30 T. Wen, X.-L. Wu, S. Zhang, X. Wang and A.-W. Xu, *Chem. - An Asian J.*, 2015, **10**, 595–601.

31 V. Eswaraiah, S. S. Jyothirmayee Aravind and S. Ramaprabhu, *J. Mater. Chem.*, 2011, **21**, 6800.

32 J. Zhu, H. Bi, Y. Wang, X. Wang, X. Yang and L. Lu, *Mater. Lett.*, 2007, **61**, 5236–5238.

33 H. Wang, J. Z. Xu, J. J. Zhu and H. Y. Chen, *J. Cryst. Growth*, 2002, **244**, 88–94.

34 A. . Ferrari, J. C. Meyer, C. Scardaci, C. Casiraghi and M. Lazzeri, *Phys. Rev. Lett.*, 2006, **97**, 187401 (4).

35 J. Cebik, J. K. McDonough, F. Peerally, R. Medrano, I. Neitzel, Y. Gogotsi and S. Osswald, *Nanotechnology*, 2013, **24**, 205703.

36 J. Chmiola, G. Yushin, Y. Gogotsi, C. Portet, P. Simon and P. L. Taberna, *Science*, 2006, **313**, 1760–3.

37 J. Huang, H. Li, Y. Zhu, Q. Cheng, X. Yang and C. Li, *J. Mater. Chem. A*, 2015, **3**, 8734–8741.

38. M. E. Plonska-Brzezinska, A. Palkar, K. Winkler and L. Echegoyen, *Electrochem. Solid-State Lett.*, 2010, **13**, K35-K38.

39. J. Breczko, K. Winkler, M. E. Plonska-Brzezinska, A. Villalta-Cerdas and L. Echegoyen, *J. Mater. Chem.*, 2010, **20**, 7761-7768.

40. M. E. Plonska-Brzezinska, J. Mazurczyk, B. Palys, J. Breczko, A. Lapinski, A. T. Dubis and L. Echegoyen, *Chem. Eur. J.*, 2012, **18**, 2600-2608.

41. E. Grądzka, K. Winkler, M. Borowska, M. E. Plonska-Brzezinska and L. Echegoyen, *Electrochim. Acta*, 2013, **96**, 274-284.

42. O. Mykhailiv, M. Imierska, M. Petelczyc, L. Echegoyen and M. E. Plonska-Brzezinska, *Chem. Eur. J.*, 2015, **21**, 5783-5793.

43. C. Xu, J. Sun and L. Gao, *J. Mater. Chem.*, 2011, **21**, 11253-11258.

Table of Contents

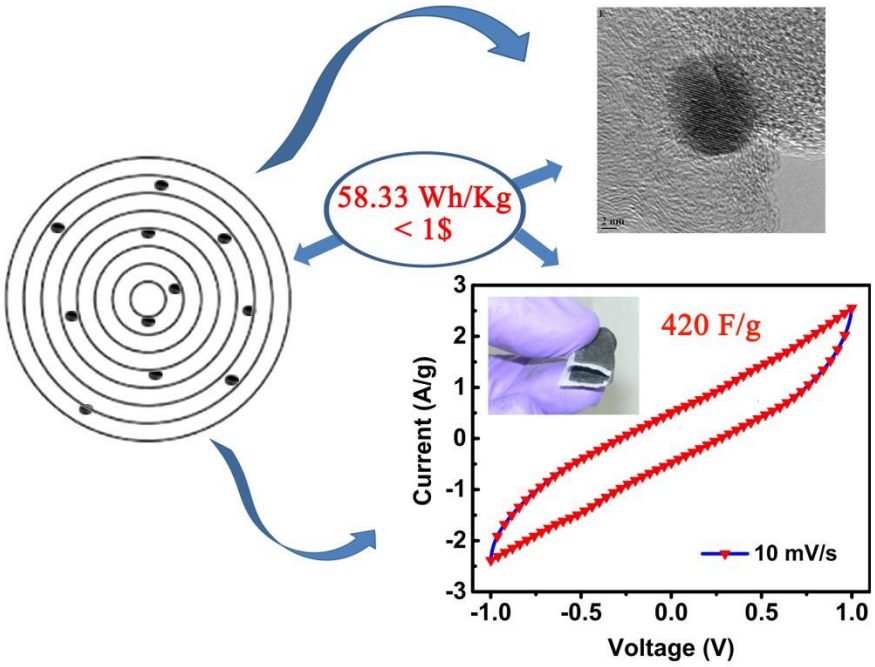

Binder-free flexible CNO-CuO composite electrodes delivering an energy density of 58.33 Wh/kg at less than 1$.